†Electronic supplementary information:

Hydrophobic Matrix-Free Graphene-Oxide Polymer Composites with Isotropic and Nematic States

Authors: Martin Wåhlander[a], Fritjof Nilsson[a], Anna Carlmark[a], Ulf W. Gedde[a], Steve Edmondson[b] and Eva Malmström[a,*]

[a]KTH Royal Institute of Technology, School of Chemical Science and Engineering, Fibre and Polymer Technology, SE-100 44 Stockholm, Sweden

[b]University of Manchester, School of Materials, Oxford Road, Manchester, M13 9PL, UK

*Corresponding author: mavem@kth.se

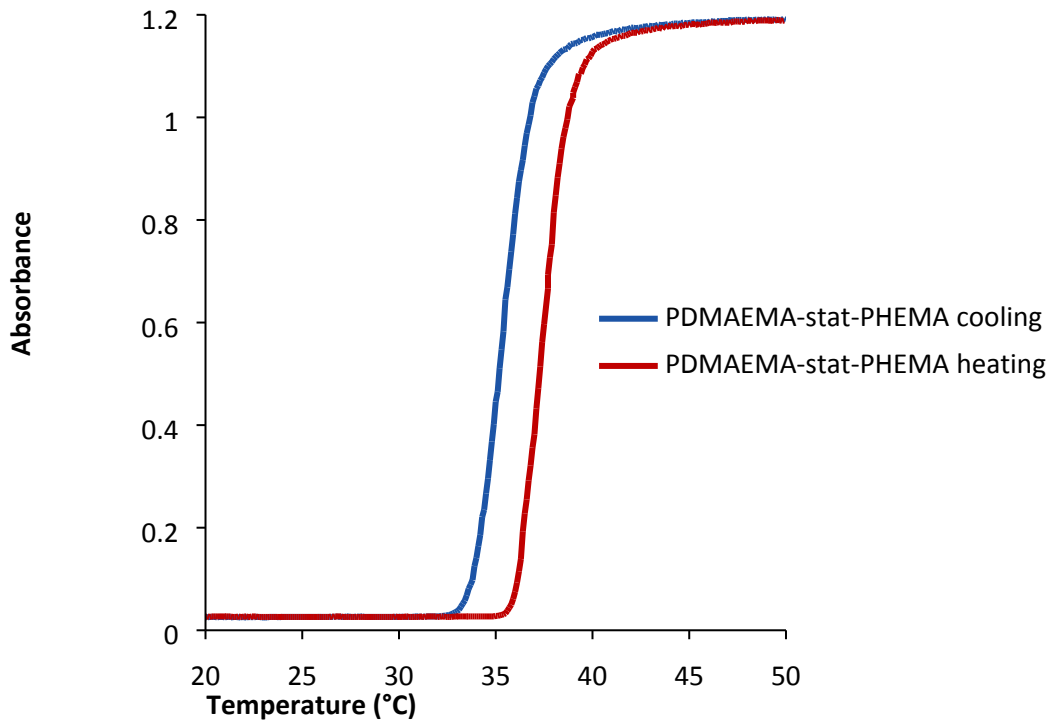

Figure S1. Representative absorbance curves of lowest critical solution temperature (LCST) of **1** PDMAEMA-*stat*-PHEMA.

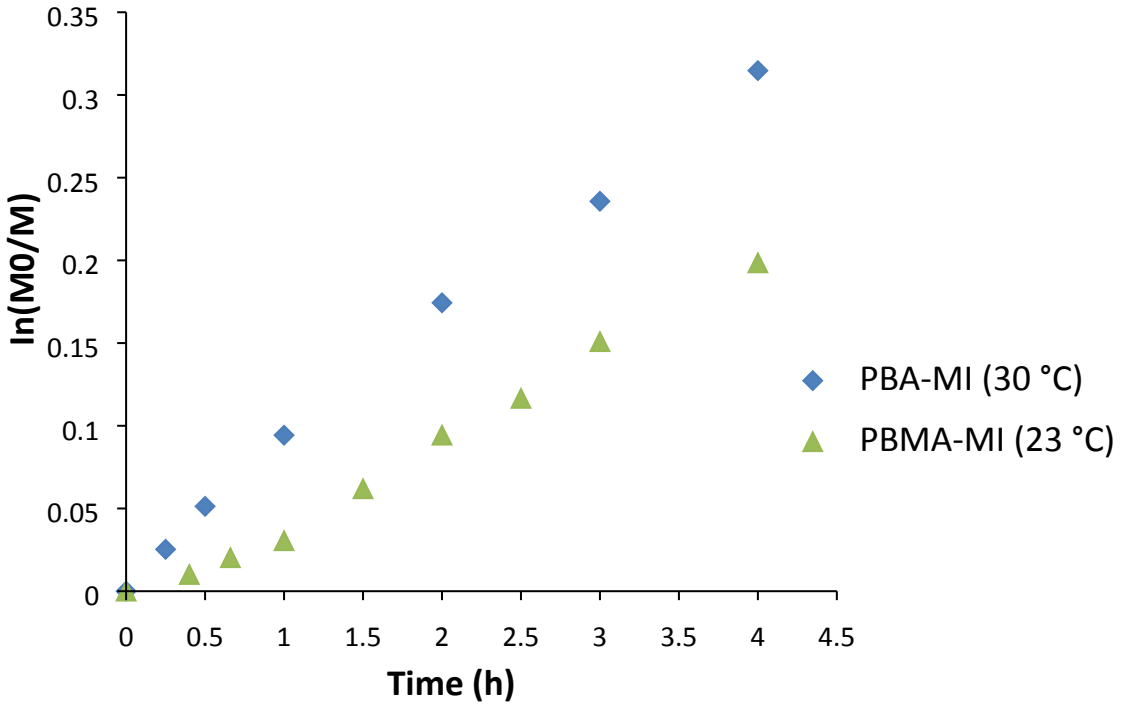

Figure S2. Representative kinetic curves of ARGET ATRPP (first order reactions) of methacrylates and acrylates initiated from free MI at 23 and 30 °C, respectively.

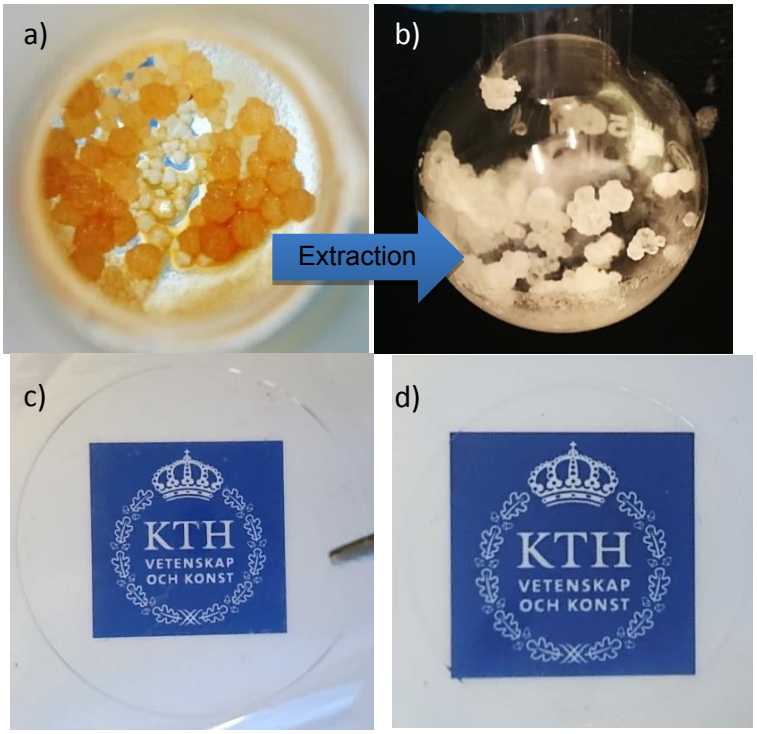

Figure S3. Precipitated aggregated beads of sticky PBA-MI a) before and b) after solvent extraction. Appearance of transparent unfilled melt-processed films (~250 µm thick) of c) linear PBMA and d) PBMA-MI.

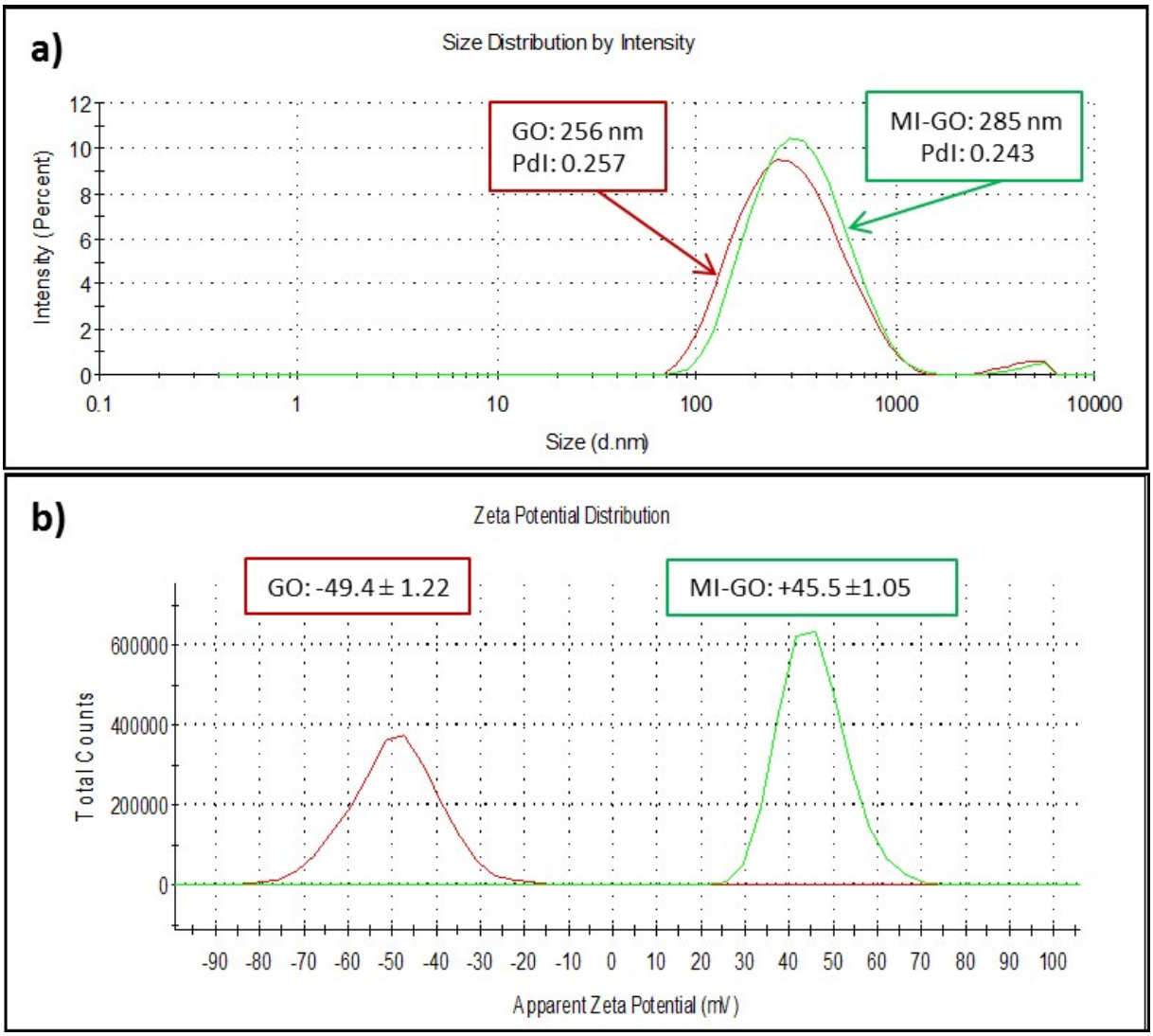

Figure S4. a) Size distributions, intensity-average sizes and PDIs of GO and MI-GO in deionized-water obtained by DLS. b) Zeta-potential of GO and MI-GO in deionized-water obtained by light scattering electrophoretic mobility measurements.

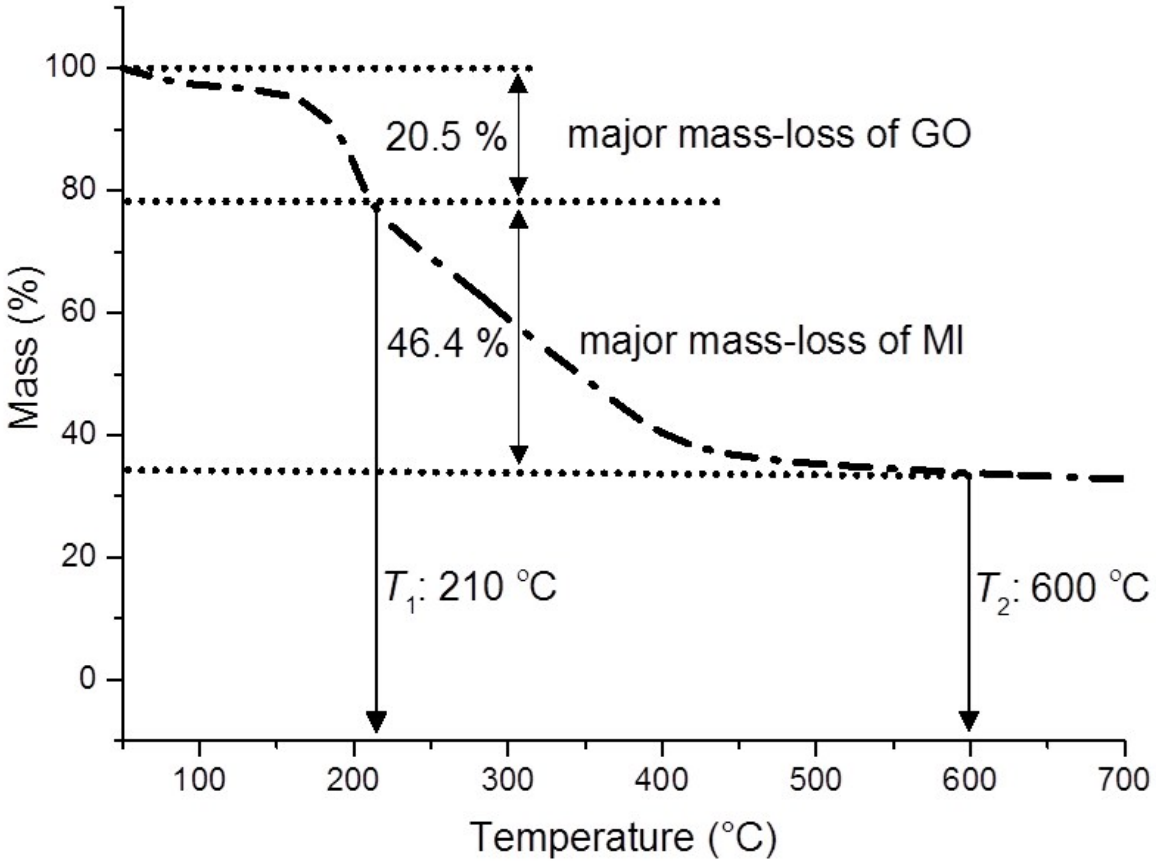

Figure S5. The mass ratio of MI-GO was roughly determined by the mass-loss in TGA above and below T_1 (210 °C). The mass loss T_1 was interpreted as being dominated by the degradation of GO. The mass loss between T_1 and T_2 (600 °C) was considered to be dominated by the degradation of MI. The mass-ratio was calculated by dividing the loss of MI (46.4%) with the loss of GO (20.5%) which equals approximately 2.3:1.0 and is in accordance to the neutralisation point of MI and GO: 2.32 ± 0.04 mg MI/mg GO.

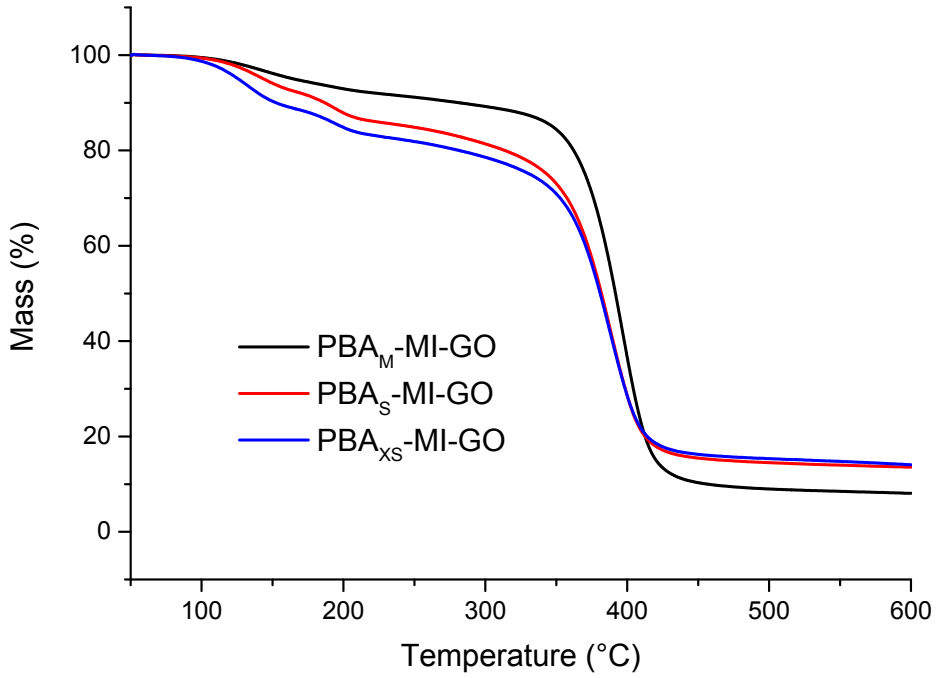

Figure S6. Thermograms of PBA-MI-GO samples showing the increased thermal stabilization with graft length, thus decreasing amount of GO and increasing time of reduction.

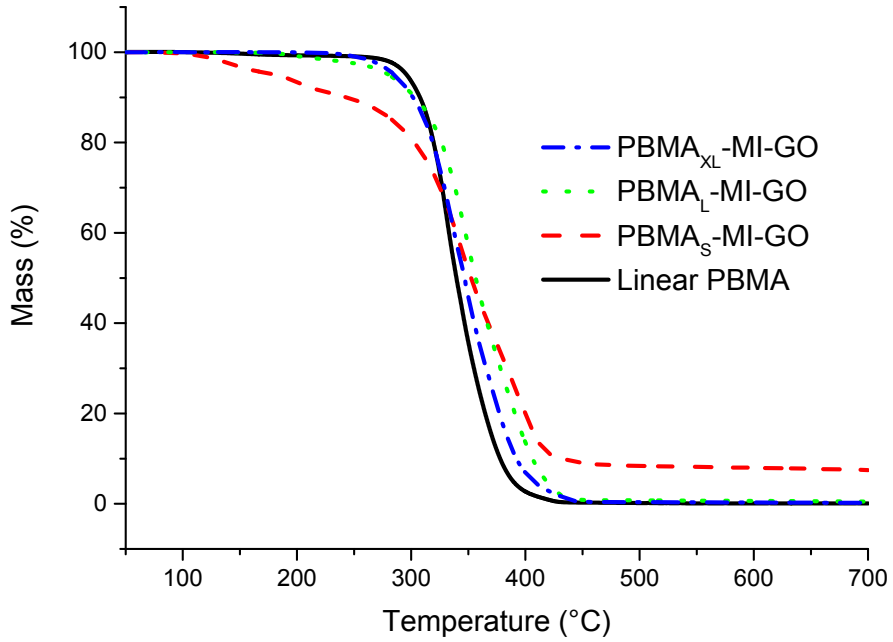

Figure S7. Thermograms of PBMA-MI-GO and linear PBMA. The thermal stability increase with graft length of PBMA-MI-GO, thus decreasing amount of GO and increasing time of reduction. The slope of decomposition gets steeper with decreasing GO content.

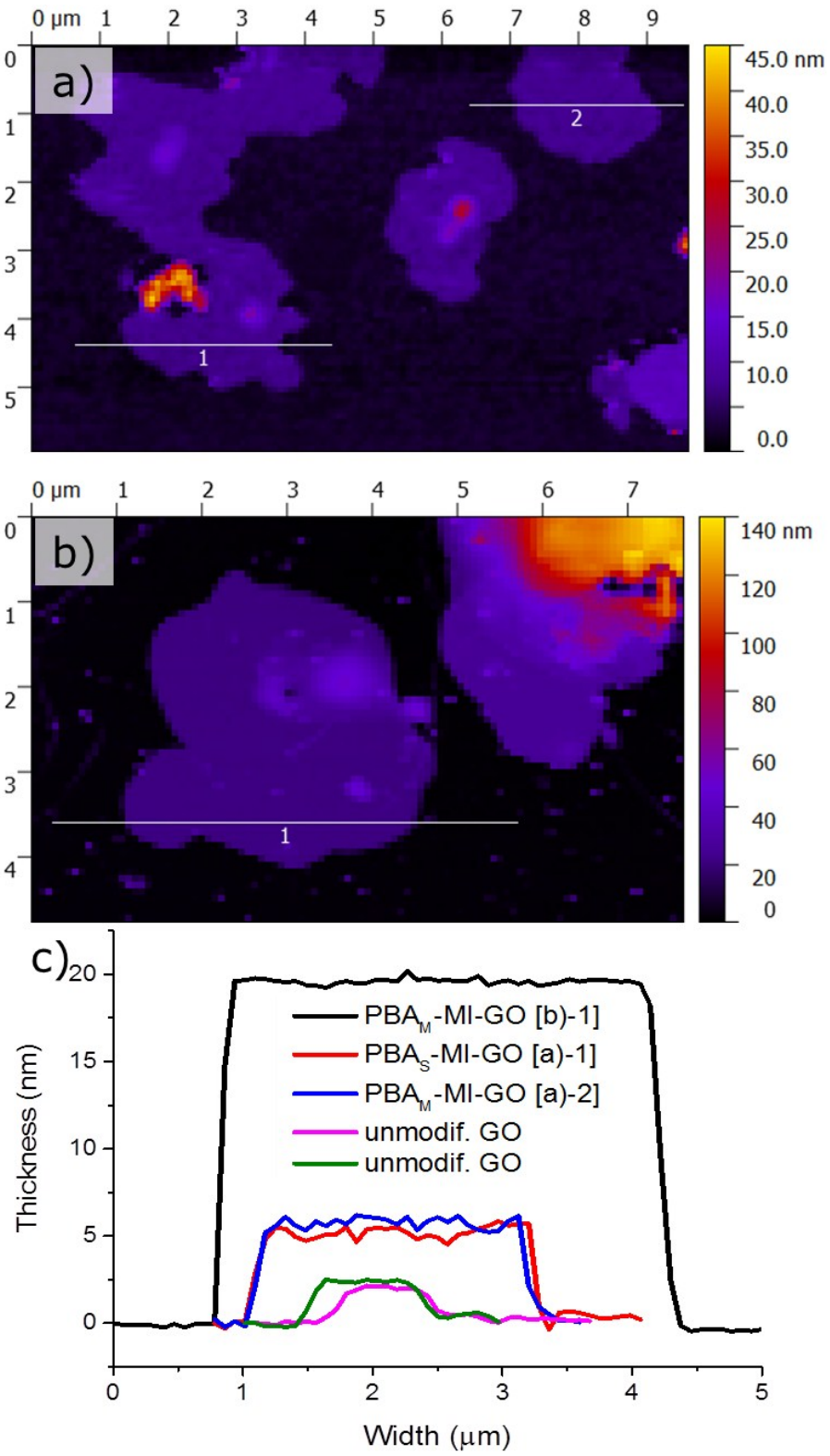

Figure S8. AFM-imaging by tapping-mode of a) PBA_S-MI-GO and b) PBA_M-MI-GO. The thickness and morphology were measured and some profiles are presented in c) representing the white lines in a) and b) marked 1 or 2. The thickness appears to be quite homogeneous for both PBA_S-MI-GO and PBA_M-MI-GO and increases with graft-length, from 2.6 ± 0.7 to 5.3 ± 0.3 nm and 17 ± 5.4 nm, respectively.

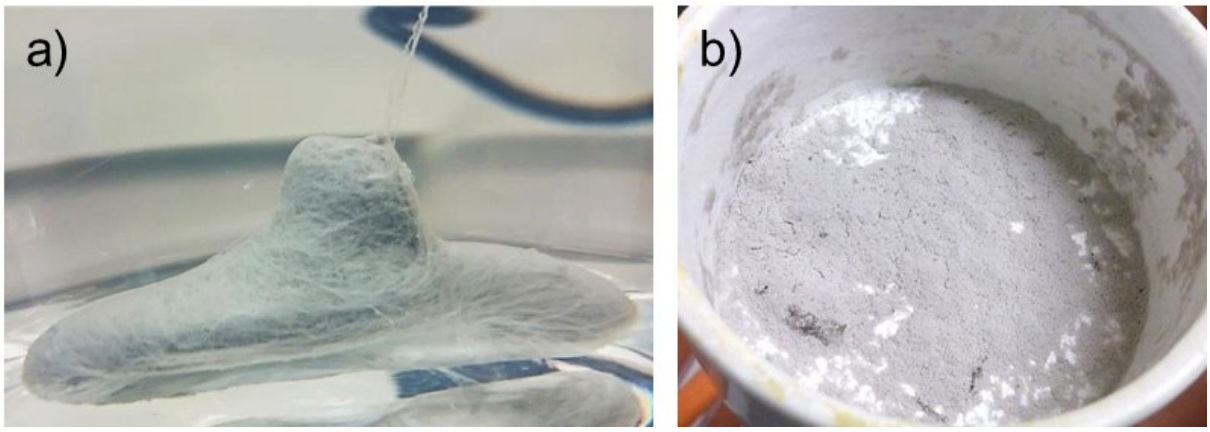

Figure S9. Precipitation of a) PBMA-MI-GO as a continuous fiber and b) PMMA-MI-GO as powder.

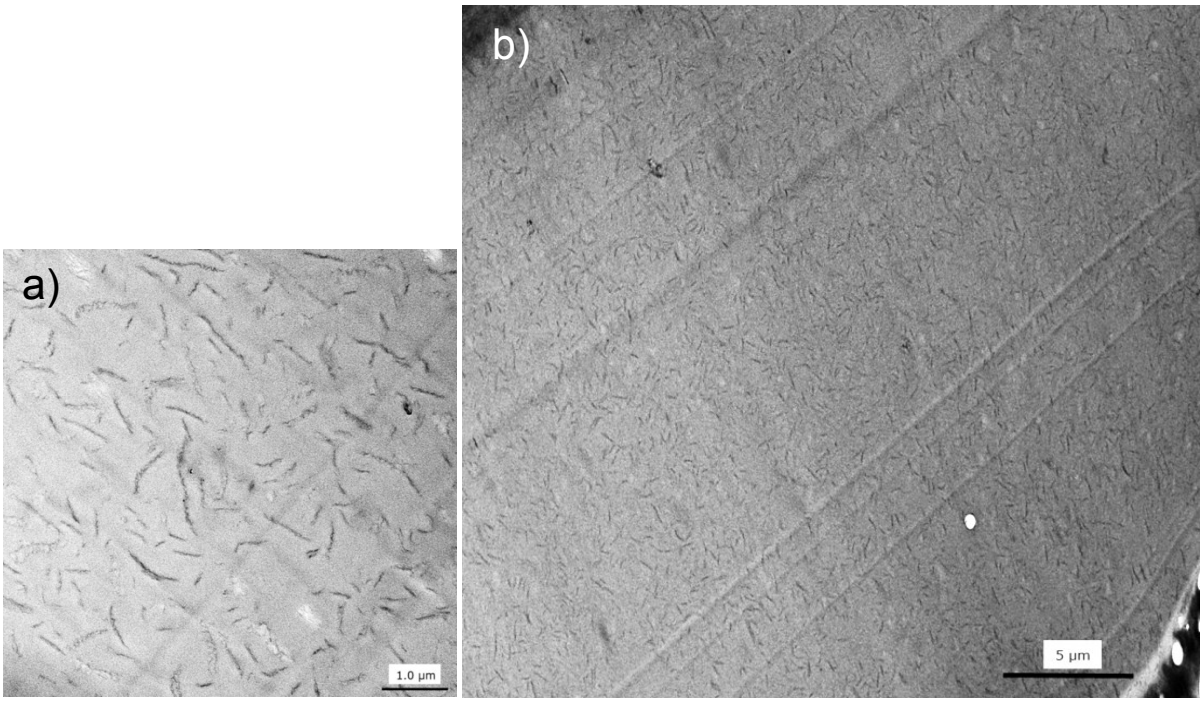

Figure S10. TEM images of the a) "state of the art" distribution of GO and b) entire microtomed sample of $PMMA_{XL}$-MI-GO providing an informative overview of the isotropic state of GO.

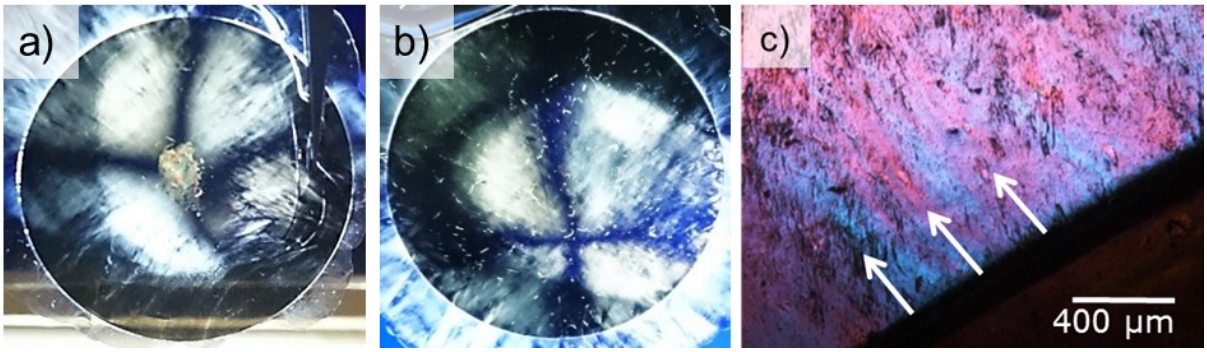

Figure S11. a),b) Giant Maltese crosses in $PMMA_{XL}$-MI-GO films (3.4 cm in diameter). c) Radial blue stripes along the direction of flow of the thin outer section of the film. The direction of flow is marked by arrows.

Table S1. Oxygen permeability and standard deviation of PBMA-MI-GO and PMMA-MI-GO films and their linear analogues (PBMA and PMMA) at 50 % and 90 % relative humidity.

Sample name	**GO ratio (vol.%)**	**OP @ RH: 50 % (90 %) (mL µm m^{-2} $24h^{-1}$ kPa^{-1})**	**Std.Dev. @ RH: 50 % (90 %)**
Linear PMMA	non	46* (49)	0.9 (0.9)
$PMMA_{XL}$-MI-GO	0.08	42 (42)	0.9 (0.4)
$PMMA_{L}$-MI-GO	0.22	48 (47)	0.2 (0.5)
$PMMA_{M}$-MI-GO	0.41	46 (48)	0.2 (0.2)
Linear PBMA	non	6000**	-
$PBMA_{XL}$-MI-GO	0.04	5700 (5800)	89.0 (69.2)
$PBMA_{L}$-MI-GO	0.28	4900 (4900)	5.7 (10.5)
$PBMA_{M}$-MI-GO	0.38	4700 (4600)	23.6 (21.4)

*Reference OP of PMMA: 56 - 92 mL µm m^{-2} $24h^{-1}$ kPa^{-1}.[18, 19 in article.] **Test failed.

Table S2. Average and standard deviation data of the storage modulus (E'), T_g at the peak of loss modulus (E''_{max}), and T_g at peak of tan δ_{peak} (E"/E') for all PMMA and PBMA containing samples.

Sample name	E' (MPa)	T_g @ E''_{max} (°C)	T_g @ tan δ_{peak} (°C)	$\tilde{M}_c$ (g mol^{-1})
Linear PMMA	2 565 ± 163	111.3 ± 1.8	126.9 ± 3.3	8 500
PMMA-MI	2 689 ± 155	123.2 ± 2.9	138.5 ± 4.5	2 200
$PMMA_M$-MI-GO	2 838 ± 220	118.5 ± 3.6	135.3 ± 3.4	5 800
$PMMA_L$-MI-GO	2 796 ± 120	119.1 ± 1.0	143.6 ± 2.1	4 400
$PMMA_{XL}$-MI-GO	2 728 ± 170	126.5 ± 1.3	144.3 ± 1.1	5 300
Linear PBMA	1 589 ± 46	29.5 ± 0.8	56.9 ± 1.3	26 000
PBMA-MI	1 315 ± 59	28.3 ± 1.8	58.2 ± 2.9	7 100
$PBMA_M$-MI-GO	1 975 ± 68	38.4 ± 0.7	58.9 ± 0.9	19 000
$PBMA_L$-MI-GO	1 762 ± 52	38.9 ± 0.8	62.5 ± 0.9	25 000
$PBMA_{XL}$-MI-GO	1 624 ± 24	39.7 ± 0.2	62.7 ± 1.7	19 000

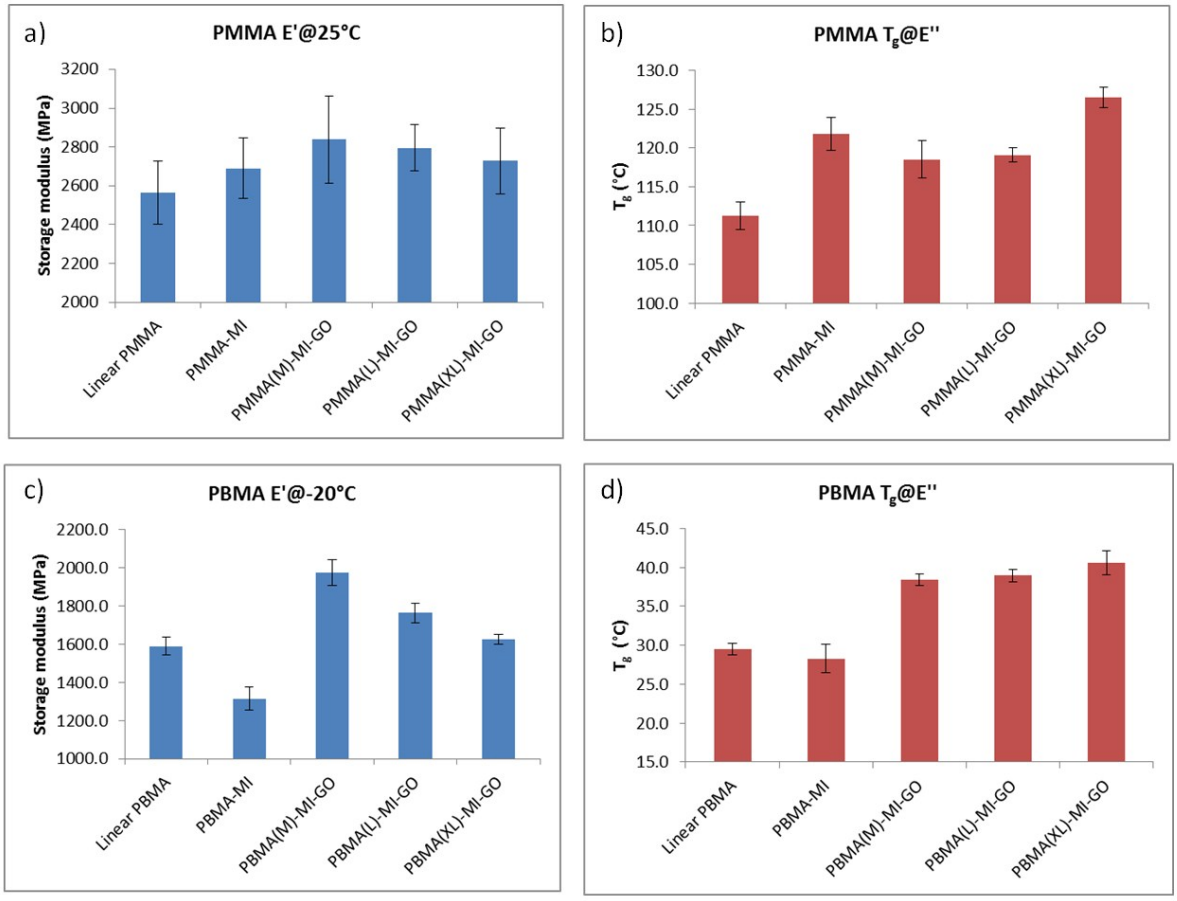

Figure S12. Graphs of the average and standard deviation data in Table S2 of the storage modulus (E') and T_g at the peak of loss modulus (T_g@E") for all a), b) PMMA and c), d) PBMA containing samples.

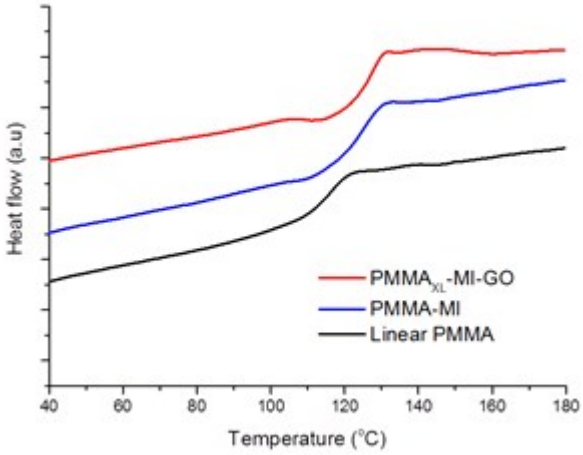

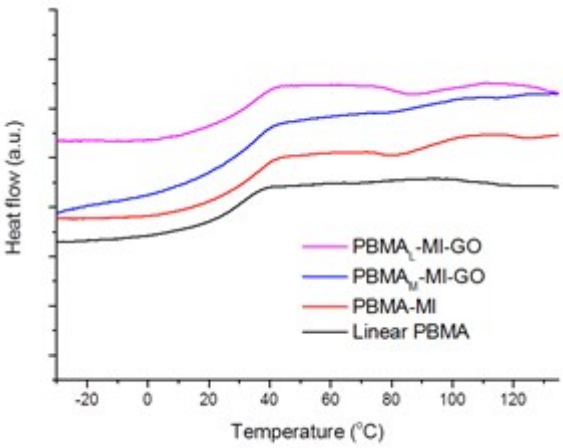

Sample name	T_g (°C)
Linear PMMA	115.8
PMMA-MI	123.7
PMMA$_{XL}$-MI-GO	126.3

Sample name	T_g (°C)
Linear PBMA	26.7
PBMA-MI	30.6
PBMA$_M$-MI-GO	31.9
PBMA$_L$-MI-GO	32.4

Figure S13. DSC curves and tabulated T_g data for linear PMMA/PBMA, PMMA-/PBMA-MI and PMMA-/PBMA-MI-GO.